COBEM 99
XV Congresso Brasileiro de Engenharia Mecânica
15th Brazilian Congress of Mechanical Engineering
22 - 26 de Novembro de 1999 / November 22 - 26, 1999 Águas de Lindóia, São Paulo,

THREE DIMENSIONAL FLOW SIMULATIONS FOR TYPICAL LAUNCH VEHICLES AT ANGLE OF ATTACK

Enda Dimitri Vieira Bigarelli
Centro Técnico Aeroespacial, Instituto Tecnológico de Aeronáutica
CTA/ITA/IEAA – 12228-900 – São José dos Campos, SP, Brasil
Olympio Achilles F. Mello
Centro Técnico Aeroespacial, Instituto de Aeronáutica e Espaço
CTA/IAE/ASA-L – 12228-904 – São José dos Campos, SP, Brasil
João Luiz F. Azevedo
Centro Técnico Aeroespacial, Instituto de Aeronáutica e Espaço
CTA/IAE/ASE-N – 12228-904 – São José dos Campos, SP, Brasil

Abstract. *Supersonic flow simulations over typical launch vehicle configurations are presented. Two different computational codes were used in this investigation. Both are 3-D finite difference codes written for general, body-conforming, curvilinear coordinate systems. The first code solves the Euler equations whereas the other code solves the Reynolds-averaged Navier-Stokes equations using a modified Baldwin-Lomax turbulence model. Simulations are performed both for the VLS and the SONDA III-A configurations at angle of attack and for various supersonic freestream Mach numbers. Computational results are validated with code-to-experiment and code-to-code comparisons.*

Keywords: *Launch vehicle, CFD, Three-dimensional flow, Flow at angle of attack, Supersonic flow.*

1. INTRODUCTION

Launch vehicles are designed to fly at very low angles of attack. Nevertheless, at the design stage, it is extremely important to determine the aerodynamics of these vehicles at angle of attack because this will provide the loads required for the structural design of the vehicle as well as the flight dynamics stability characteristics necessary for control system design. Zdravistch and Azevedo (1990) have performed axisymmetric viscous simulations for flows over the VLS with very good representation of the flow physics. Moreover, three-dimensional inviscid computations over the VLS at low angles of attack with good agreement with experimental data were also performed by Azevedo, Zdravistch and Silva (1991) and Azevedo *et al.* (1996).

Two different computational codes were used for simulations of VLS and SONDA III-A flows at angle of attack and for various supersonic freestream Mach numbers. Both solvers are 3-D finite difference codes written for general, body-conforming, curvilinear coordinate systems. The first code, denominated *SolverA* in the present work, solves the compressible Euler equations. The other code, *SolverB*, solves the Reynolds-averaged Navier-Stokes equations using a modified Baldwin-Lomax turbulence model.

The problem of simulating supersonic flows over such a complex vehicle as the VLS or SONDA III-A is not a new requirement at IAE. *SolverB* was an already existing code at the Institute. It was developed for aircraft wing applications and later modified for launch vehicle configurations. It has been used for several different configurations and, although quite reliable, it has many cumbersome code portions associated with its original conception for aircraft applications. The authors felt that these problems might preclude further improvements in the present simulation capability. Therefore, there were reasons to develop a newer code with an unified programming style and with more powerful data structures to allow the future implementation of the capability to handle more complex launch vehicle configurations.

Since experimental data is available only for the VLS configuration, computations were made with *SolverB* for VLS at freestream Mach number of 1.25 and angle of attack of 0 deg. Results for these calculations were compared to the experimental data in order to assess the code effectiveness in the solution for the present aerospace configurations. Both solvers were used to simulate flows over the SONDA III-A at freestream Mach numbers of 1.25 and 2.00 and angle of attack of 0 and 2 deg. The computational results were used for a code-to-code comparison. The capability implemented is used to further assess the aerodynamic characteristics at angle of the VLS and other vehicles currently considered at IAE.

2. THEORETICAL FORMULATION

SolverA solves the three-dimensional, compressible Euler equations. These equations can be written in strong conservation-law form for general, body-conforming, curvilinear coordinates (Pulliam and Steger, 1980, and Azevedo, Zdravistch and Silva, 1991) as

$$\frac{\partial \overline{Q}}{\partial \tau} + \frac{\partial \overline{E}}{\partial \xi} + \frac{\partial \overline{F}}{\partial \eta} + \frac{\partial \overline{G}}{\partial \zeta} = 0 \ . \tag{1}$$

The vector of conserved quantitites, $\overline{Q}$, can be defined as

$$\overline{Q} = J^{-1} \left[\begin{array}{ccccc} \rho & \rho u & \rho v & \rho w & e \end{array} \right]^{\mathrm{T}} \ , \tag{2}$$

and the inviscid flux vectors, $\overline{E}$, $\overline{F}$ and $\overline{G}$, can be written as

$$\overline{E} = J^{-1} \left\{ \begin{array}{c} \rho U \\ \rho u U + p \xi_x \\ \rho v U + p \xi_y \\ \rho w U + p \xi_z \\ (e+p) U - p \xi_t \end{array} \right\} \ , \qquad \overline{F} = J^{-1} \left\{ \begin{array}{c} \rho V \\ \rho u V + p \eta_x \\ \rho v V + p \eta_y \\ \rho w V + p \eta_z \\ (e+p) V - p \eta_t \end{array} \right\} \ ,$$

$$\overline{G} = J^{-1} \left\{ \begin{array}{c} \rho W \\ \rho u W + p \zeta_x \\ \rho v W + p \zeta_y \\ \rho w W + p \zeta_z \\ (e+p) W - p \zeta_t \end{array} \right\} \ . \tag{3}$$

In the usual nomenclature, being adopted in the present work, ρ is the density, u, v and w are the Cartesian velocity components, p is the pressure, and e is the total energy per volume unity. The pressure is obtained from the equation of state for perfect gases, written as

$$p = (\gamma - 1) \left[e - \frac{1}{2} \rho \left(u^2 + v^2 + w^2 \right) \right] \ , \tag{4}$$

where γ is the ratio of specifics heats. The contravariant velocity components, U, V and W, can be written as

$$\begin{aligned} U &= \xi_t + \xi_x u + \xi_y v + \xi_z w \ , \\ V &= \eta_t + \eta_x u + \eta_y v + \eta_z w \ , \\ W &= \zeta_t + \zeta_x u + \zeta_y v + \zeta_z w \ . \end{aligned} \tag{5}$$

Expressions for the Jacobian of the transformation, J, and for the various metric terms can be found in Pulliam and Steger (1980), among other references.

SolverB solves the three-dimensional Reynolds-averaged Navier-Stokes (RANS) equations. The solver was adapted from the method developed by Sankar and Kwon (1990). The vector form of the full 3-D RANS equations based on an arbitrary curvilinear coordinate system can be written in non-dimensional form as

$$\frac{\partial \overline{Q}}{\partial \tau} + \frac{\partial \overline{E}}{\partial \xi} + \frac{\partial \overline{F}}{\partial \eta} + \frac{\partial \overline{G}}{\partial \zeta} = \frac{1}{Re}\left(\frac{\partial R}{\partial \xi} + \frac{\partial S}{\partial \eta} + \frac{\partial T}{\partial \zeta}\right) \tag{6}$$

where $\overline{Q}$ is the vector of unknown flow properties; $\overline{E}$, $\overline{F}$, $\overline{G}$ are the inviscid flux vectors; R, S, T are the viscous flux vectors and $Re = \rho_\infty a_\infty d/\mu_\infty$ is the Reynolds number based on the free-stream speed of sound a_∞, density ρ_∞, viscosity μ_∞ and reference length d.

3. NUMERICAL IMPLEMENTATION

For *SolverA* the governing equations were discretized in a finite difference context. The spatial discretization adopted uses a central difference type algorithm plus explicity added artificial dissipation terms in order to control nonlinear instabilities. The equations, fully discretized in space, can be written as

$$\left(\frac{\partial \overline{Q}}{\partial \tau}\right)_{i,j,k} = -\mathrm{RHS}_{i,j,k} \ . \tag{7}$$

The right-hand side operator of Eq. (7) is defined as

$$\begin{aligned} \mathrm{RHS}_{i,j,k} &= \frac{1}{2\,\Delta\xi}\left(\overline{E}_{i+1,j,k} - \overline{E}_{i-1,j,k}\right) + \frac{1}{2\,\Delta\eta}\left(\overline{F}_{i,j+1,k} - \overline{F}_{i,j-1,k}\right) \\ &+ \frac{1}{2\,\Delta\zeta}\left(\overline{G}_{i,j,k+1} - \overline{G}_{i,j,k-1}\right) \ , \end{aligned} \tag{8}$$

where $\Delta\xi = \Delta\eta = \Delta\zeta = 1$ for the general curvilinear coordinate case.

An anisotropic scalar artificial dissipation method, as described in Turkel and Vatsa (1994), was used. This scheme is nonlinear and allows a connection between artificial dissipation terms of second and fourth order, which is very important in capturing shock waves through the flow.

Time march uses an explicit, second order, five-stages Runge-Kutta scheme, as seen at Jameson and Mavriplis (1986), and Jameson, Schmidt and Turkel (1981), which can be written as

$$\begin{aligned} \overline{Q}^{(0)}_{i,j,k} &= \overline{Q}^{n}_{i,j,k} \ , \\ \overline{Q}^{(\ell)}_{i,j,k} &= \overline{Q}^{(0)}_{i,j,k} - \alpha_\ell\, \Delta t_{i,j,k}\, \mathrm{RHS}^{(\ell-1)}_{i,j,k} \ , \qquad \ell = 1,2,\ldots,5, \\ \overline{Q}^{n+1}_{i,j,k} &= \overline{Q}^{(5)}_{i,j,k} \ . \end{aligned} \tag{9}$$

In the previous expressions, Δt stands for the time step, and n and $n+1$ are the property values at the start and at the end of each time step.

For the configurations under consideration here, the types of boundary conditions that should be considered include solid walls, far field boundaries, upstream centerline and downstream (exit) conditions. For the rocket wall, zero-order extrapolation of the conserved variables from the computational plane near the wall was used in order to obtain the boundary data. The upstream centerline is a singularity of the coordinate transformation and, hence, an adequate treament of this boundary must be provided. In the present case, the approach consisted in extrapolating the property values from the adjacent longitudinal plane and in averaging the extrapolated values in the azimuthal direction in order to define the updated properties at the upstream centerline. At the exit plane, the boundary conditons were implemented through the

use of the 1-D characteristic relations for the 3-D Euler equations. The interested reader is referred to the work of Azevedo, Fico and Ortega (1995) for further details on the use of 1-D characteristic relations for boundary condition implementation. Finally, freestream properties are assumed at the far field boundaries.

For *SolverB* the time derivative, $\overline{Q}_\tau$, of Eq. (6) is approximated using two-point backward difference at the new time level $n+1$. All spatial derivatives are approximated by standard second-order central differences and are represented by the difference operator δ. The streamwise and normal derivatives, $\overline{E}_\xi$ and $\overline{G}_\zeta$, are evaluated implicitly at the new time level $n+1$. The azimuthal derivative, $\overline{F}_\eta$, is evaluated explicitly at the old time level n but uses the $n+1$ values as soon as they become available. This semi-explicit treatment of the azimuthal derivative enables the scheme to solve implicitly for $\Delta\overline{Q}^{n+1}$ at all points at a given η-plane at a time. To eliminate any dependency the solution may have on the sweeping direction, the solver reverses the direction of azimuthal sweeping with every sweep. The viscous terms R_ξ, S_η and T_ζ are evaluated explicitly, using half-point central differences denoted here by the difference operator $\bar{\delta}$, so that the computational stencil for the stress terms uses only three nodes in each of the three directions. Explicit treatment of the stress terms still permits the use of large time steps since the Reynolds numbers of interest here are fairly large. With the above described time and space discretizations, Eq. (6) becomes

$$\Delta\overline{Q}^{n+1} + \Delta\tau\left(\delta_\xi\overline{E}^{n+1} + \delta_\eta\overline{F}^{n,n+1} + \delta_\zeta\overline{G}^{n+1}\right) = \frac{\Delta\tau}{Re}\left(\bar{\delta}_\xi R^{n,n+1} + \bar{\delta}_\eta S^{n,n+1} + \bar{\delta}_\zeta T^{n,n+1}\right) \quad (10)$$

Application of Eq. (10) to the grid points leads to a system of non-linear, block penta-diagonal matrix equations for the unknown $\Delta\overline{Q}^{n+1} = \overline{Q}^{n+1} - \overline{Q}^n$, since the convection fluxes $\overline{E}$, $\overline{F}$, $\overline{G}$ are non-linear functions of the vector of unknown flow properties $\overline{Q}$. Equation (10) is then linearized using the Jacobian matrices $A = \partial\overline{E}/\partial\overline{Q}$ and $C = \partial\overline{G}/\partial\overline{Q}$. This results in a system of linear, block penta-diagonal matrix equations, which is considerably expensive to solve. The approach used here is to employ an approximate factorization and the diagonal algorithm of Pulliam and Chaussee (1981), to diagonalize A and C. This approach yields

$$T_\xi^n\left[I + \Delta\tau\delta_\xi\Lambda_\xi^n\right]N^n\left[I + \Delta\tau\delta_\zeta\Lambda_\zeta^n\right]\left(T_\zeta^{-1}\right)^n\Delta\overline{Q}^{n+1} = \mathrm{RHS}^{n,n+1} \quad (11)$$

The solution of Eq. (11) involves two block-tridiagonal systems where the blocks are diagonal matrices. The use of standard central differences to approximate the spatial derivatives can give rise to the growth of high frequency errors in the numerical solution with time. To control this growth, a set of 2nd/4th order non-linear, spectral radius based, explicit artificial dissipation terms are added to the discretized equations. A slightly modified version of the Baldwin and Lomax (1978) algebraic turbulence model is used, where the maximum shear stress is used instead of the wall shear stress because in the vicinity of separation points, the shear stress values approach zero at the wall.

The meshes used by the two numerical codes were adapted from a 2-D grid. The procedure was as follows: a computational grid used previously for axisymetric computations was rotated so as to generate a 3-D grid around half of the body. For *SolverA*, one more plane was added, before and after the symmetry plane, where each ζ-plane corresponds to a longitudinal plane. Symmetry boundary conditions were used for these two extra planes. The resulting grid for *SolverA* had $156\times34\times21$ points (Fig. 1). The grid used by *SolverB* had $155\times19\times65$ points.

4. RESULTS AND DISCUSSION

A comparison of the computational results obtained with *Solver B* and experimental data obtained with wind tunnel tests can be seen in Fig. 2. This figure considers the VLS at freestream conditions $M_\infty = 1.25$ and $\alpha = 0$ deg. It presents Cp distributions at two different longitudinal

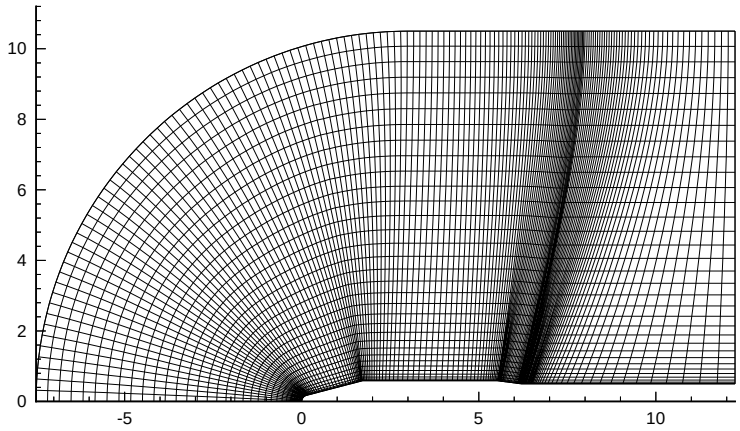

Figure 1: Overall view of a plane from the SONDA III-A 3-D grid used with *SolverA*.

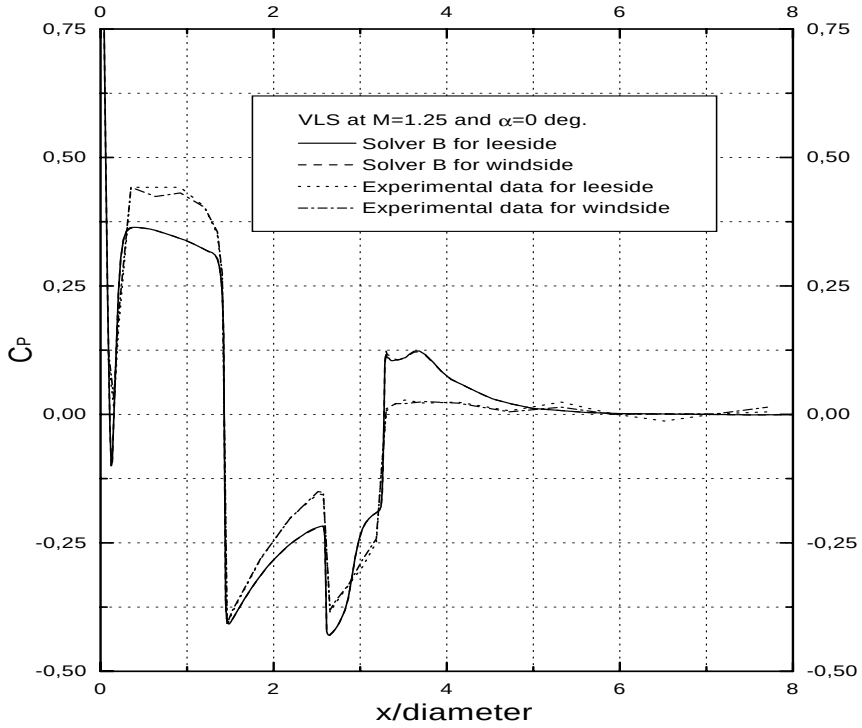

Figure 2: Numerical results with *SolverB* compared to experimental data for VLS at $\alpha = 0$ deg. and $M_\infty = 1.25$.

planes, which are the vehicle leeward and windward generators. The results show that the solution with both experimental treatment and computational simulation for the two opposite planes do not present differences, which is the expected result at $\alpha = 0$ deg. One can observe in Fig. 2 that, although experimental and computational results follow the same trends, there are a few discrepancies in the Cp distributions. Fortunately, for actual applications in design, one is typically concerned with the running normal loads and not with the local pressure distributions. Hence, circumferencial integrations of the pressure distributions tend to cancel out the effect of the discrepancies in the local pressures, yielding a much better agreement between experiment and computation (Mello and Azevedo, 1998).

Several other results are available for flow simulation over the VLS using *Solver B*. However, the comparison shown in Fig. 2 is already sufficient to indicate the level of agreement which can be obtained with the experimental data by this code. Moreover, these results are representative of the quality of the numerical solutions obtained with the code throughout the speed range analyzed. It is interesting to observe that, since the VLS is the most important vehicle under development in the space sector of IAE, there were quite extensive wind tunnel tests performed for this vehicle. Hence, a fairly large amount of experimental data is available for this vehicle, at least in terms of wall pressure distributions and integrated force and moment data.

However, several other vehicles are currently being developed, or improved, within the range of responsibilities of the Institute. Due to obvious budgetary constraints in the country, it is not always possible to take these other vehicles to the wind tunnel, especially because this would usually mean performing the tests overseas. Therefore, the CFD simulation capability available at the group should be able to perform reliable calculations for general rocket-like configurations which will fly without ever being in a wind tunnel. In particular, at present, there is strong interest in performing calculations for the vehicle denoted SONDA III-A, which is a modified version of an existing sounding rocket. Since no experimental data are available for the SONDA III-A, the calculations are performed with two different codes and code-to-code comparisons are used to assess the correctness of the numerical results.

Pressure coefficient distributions for flow over the SONDA III-A at freestream Mach number $M_\infty = 1.25$ and at zero degree angle of attack are shown in Fig. 3. This figure includes the Cp distributions at two different longitudinal planes, namely, for the vehicle leeward and windward generators, calculated with the two computational codes here discussed. The results show that the solution with the same code for the two opposite planes do not present differences, which is the expected result at $\alpha = 0$ deg. However, there are a few discrepancies between results with different codes. In particular, one can observe a fairly large number of oscillations for the $SolverA$ solution, whereas $SolverB$ results are a lot smoother. Apparently, the observed oscillations can be attributed to the lower levels of artificial dissipation present in $SolverA$. On the other hand, this lower dissipation level allowed a more accurate capture of the shock wave at the boattail-afterbody cylinder intersection, as one can clearly see in Fig. 3. Unfortunately, this crisp shock resolution is accompanied by strong pre-shock and post-shock oscillations. On the other hand, solutions with *Solver B* do not have oscillations, but they present a much more smeared shock solution. Nevertheless, the overall features of the flow are well captured by both solutions and, as expected, the pressure distribution downstream of the boattail-afterbody cylinder shock drops smoothly to the freestream condition.

Similar results for the SONDA III-A at angle of attack, with $\alpha = 2$ deg., are shown in Fig. 4. As in the previous case, the freestream Mach number is $M_\infty = 1.25$ and the figure shows the pressure coefficient distributions at the leeside and windside calculated with the two different codes. The results are indicating that the two codes obtain essentially the same solution for the corresponding azimuthal planes. In this case, since a positive angle of attack is considered, one can observe that the windside pressures are higher than the leeside ones, as expected. In general, the same trends observed in the results presented in Fig. 3 can also be seen in this case with regard to the rather oscillatory behavior of *Solver A* solution. Furthermore, the boattail-

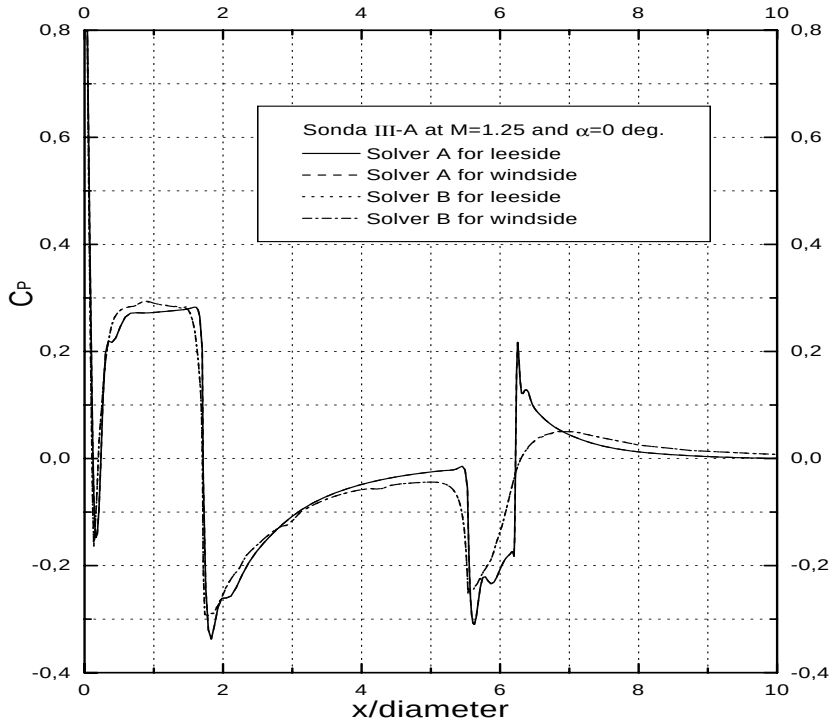

Figure 3: Pressure coefficient distribution over the SONDA III-A at $\alpha = 0$ deg. and $M_\infty = 1.25$.

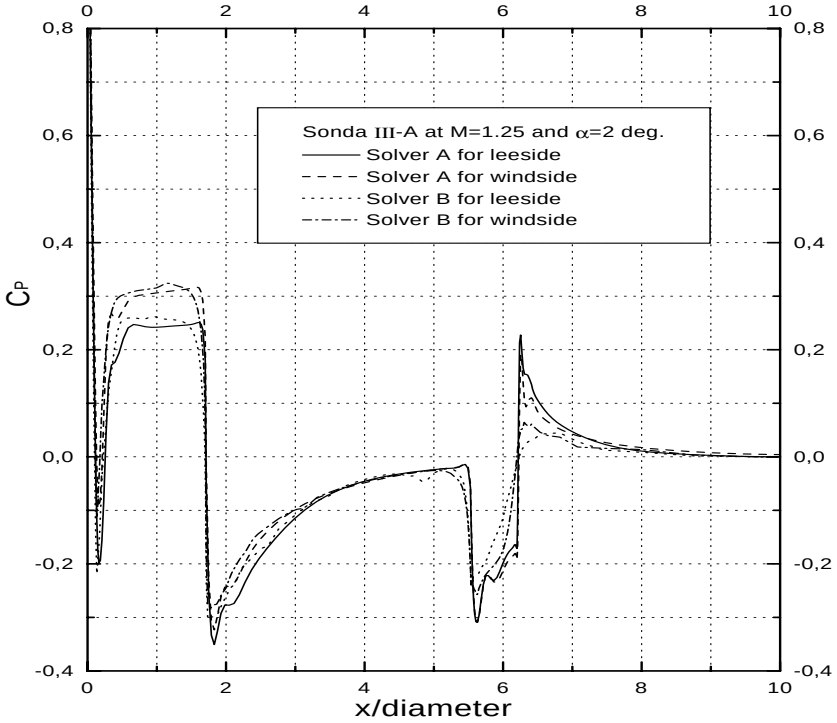

Figure 4: Pressure distribution over the SONDA III-A at $\alpha = 2$ deg. and $M_\infty = 1.25$.

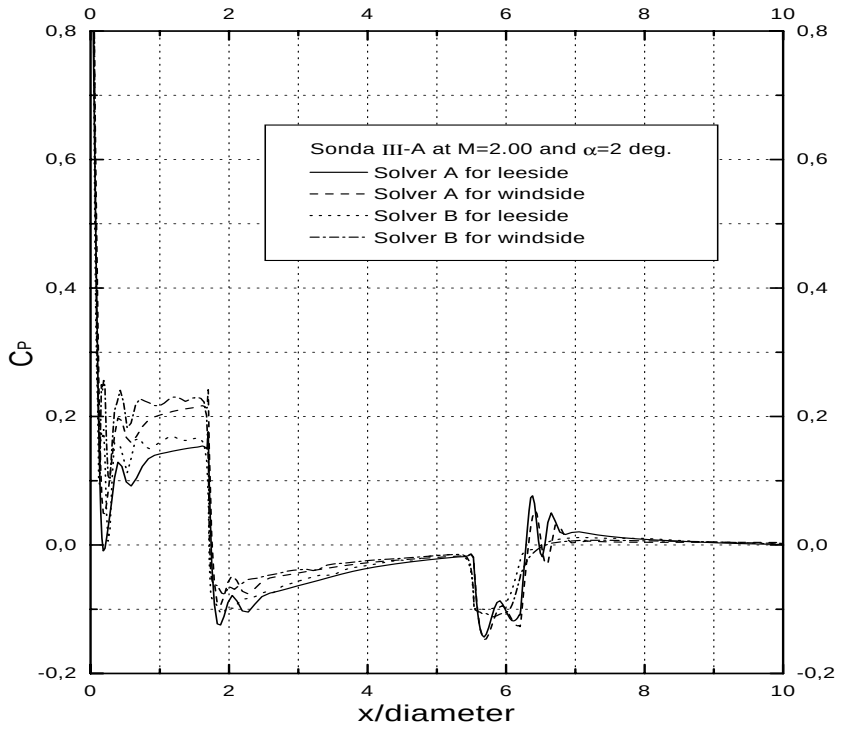

Figure 5: Pressure distribution over the SONDA III-A at $\alpha = 2$ deg. and $M_\infty = 2.00$.

afterbody cylinder intersection shock resolution is a lot crisper with this code, as also observed in the previous results. One can also observe that most of the oscillations in the *Solver A* solution are present in the boattail region and in the upstream portion of the afterbody cylinder. Hence, the solution in the front part of the vehicle is a lot smoother. Moreover, if one was interested in integrated forces and moments, the integration of the different distributions obtained with the two codes would yield an even better comparison of the calculation results.

Results for a higher freestream Mach number, $M_\infty = 2.00$, are presented in Fig. 5 for the case of the SONDA III-A at $\alpha = 2$ deg. As before, both leeside and windside pressure coefficients are presented in the figure for the two computational codes available. This case has stronger shock waves present in flow and, hence, it is a more challenging test case for both codes. One can observe, however, that the features of the flow are well captured by both solutions. The same curve patterns seen at Figs. 3 and 4 are observed in this figure as well. The influence of the dissipation terms on the numerical solution can be again verified. The general conclusion that can be drawn from the comparison of these curves is that *Solver B* seems to be adding considerably larger amounts of artificial dissipation into the numerical solution.

These results demonstrated a good agreement between the two solvers. Small differences appeared due to numerical errors and dissipative terms. Comparisons made between the results of $SolverB$ for VLS and experimental data showed the level of agreement between the numerical solution and the experimental data. Therefore, since comparisons made between the two numerical solutions showed that results for $SolverA$ are in good agreement with those of $SolverB$, one can accept that the implementation of *Solver A* was successfully accomplished. Hence, as a way of acquiring further understanding of the results for the SONDA III-A vehicle, the forthcoming figures present flow visualizations of the solutions obtained with *Solver A*. Hence, Fig. 6 shows the Mach number contours for the case with freestream conditions of $M_\infty = 2.00$ and $\alpha = 2$ deg. Similar results in terms of dimensionless pressure contours for $M_\infty = 1.25$ and $\alpha = 2$ deg.

are presented in Fig. 7. Results showed good accuracy of the solver at capturing shock waves throughout the flowfield, and the shock pattern is in very good agreement with theory.

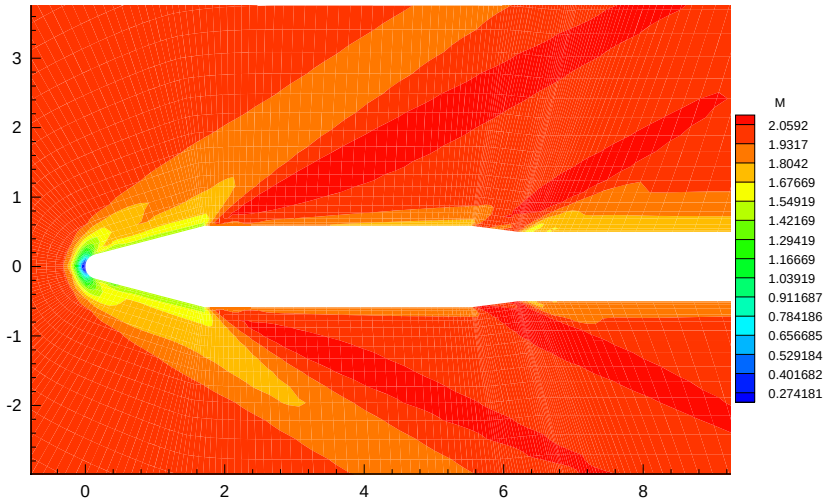

Figure 6: Mach number contours for SONDA III-A at $\alpha = 2$ deg. and $M_\infty = 2.00$.

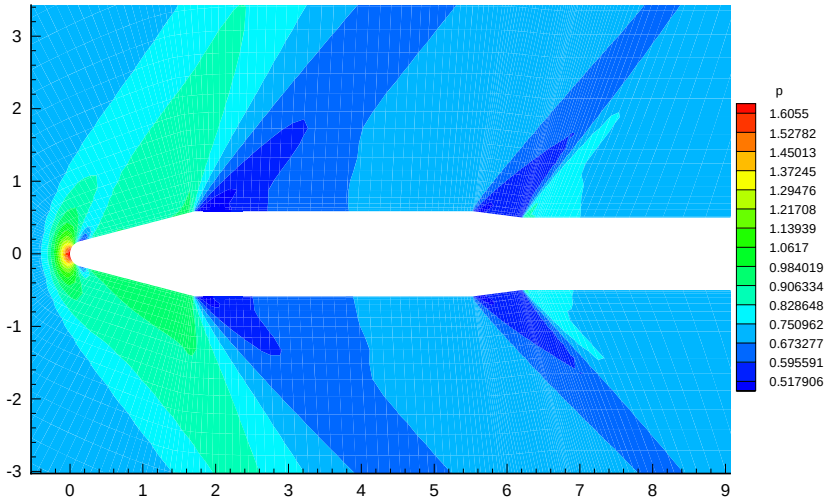

Figure 7: Dimensionless pressure contours for SONDA III-A at $\alpha = 2$ deg. and $M_\infty = 1.25$.

5. CONCLUDING REMARKS

This work presented an effort to validate a new computational code which solves the three-dimensional, compressible Euler equations in strong conservation-law form for general, body-conforming, curvilinear coordinates. Due to requirements at IAE of solving the flow over complex aerospace configurations and to the fact that the original concept of the already existing solver ($SolverB$) was not initially headed to this kind of configuration, a new solver ($SolverA$) made itself necessary. The validation effort involved the comparison of numerical results for the old solver with available experimental data and the comparison of numerical results from the new solver to the old one.

Simulations with $SolverB$ for the VLS at $M = 1.25$ and $\alpha = 0$ deg. were performed, since available experimental data could only be found for this configuration. Numerical and

experimental results showed the level of agreement between the two methods. Furthermore, calculations with the two solvers under consideration in this work were performed for the SONDA III-A vehicle at various supersonic freestream Mach numbers and at angle of attack. Results showed good agreement between the numerical solutions. The effect of artificial dissipation terms was observed at the results. The results also indicate that there is a need for further validation and calibration of *Solver A*. However, the good agreement between the two numerical solutions are an indication that *SolverA* has the correct capabilities to support any further development for addressing flows over more complex launch vehicles and to handle the requirements of interest at IAE.

Acknowledgments

The present work was partially supported by Conselho Nacional de Desenvolvimento Científico e Tecnológico, CNPq, under the Integrated Project Research Grant No. 522413/96-0.

REFERENCES

Azevedo, J.L.F., Fico, N.G.C.R.., Jr., and Ortega, M.A., 1995, Two-dimensional and axisymmetric nozzle flow computations using the Euler equations, Journal of the Brazilian Society of Mechanical Sciences, Vol. 17, No. 2, pp. 147-170.

Azevedo, J.L.F., Moraes, P., Jr., Maliska, C.R., Marchi, C.H., and Silva, A.F.C., 1996, Code validation for high-speed flow simulation over satellite launch vehicle, Journal of Spacecraft and Rockets, Vol. 33, No. 1, pp. 15-21.

Azevedo, J.L.F., Zdravistch, F., and Silva, A.F.C., 1991, Implementation and validation of Euler solvers for launch vehicle flows, Proceedings of the Fourth International Symposium on Computational Fluid Dynamics, Vol I, Davis, CA, September, pp. 42-47.

Baldwin, B.S., and Lomax, H., 1978, Thin layer approximation and algebraic model for separated turbulent flows, AIAA Paper 78-257, January, Palo Alto, CA.

Jameson, A., and Mavriplis, D., 1986, Finite Volume Solution of the Two-Dimensional Euler Equations on a Regular Triangular Mesh, AIAA Journal, Vol. 24, No. 4, pp. 611-618.

Jameson, A., Schmidt, W., and Turkel, E., 1981, Numerical solution of the Euler equations by finite volume methods using Runge-Kutta time-stepping schemes, AIAA Paper 81-1259, AIAA 14th Fluid and Plasma Dynamics Conference, June, Palo Alto, CA.

Mello, O.A.F., and Azevedo, J.L.F., 1998, Calculation of the aerodynamic loads over the VLS central body at high angles of attack, Report NT-157/ASE-N/98, Instituto de Aeronaáutica e Espaço, SP (in Portuguese).

Pulliam, T.H., and Chaussee, D.S., 1981, A diagonal form of an implicit approximate-factorization algorithm, Journal of Computational Physics, Vol. 39, pp. 347-363.

Pulliam, T.H., and Steger, J.L., 1980, Implicit finite-difference simulations of three-Dimensional compressible flow, AIAA Journal, Vol. 18, No. 2, pp. 159-167.

Sankar, L.N., Kwon, O.J., 1990, High-alpha simulation of fighter aircraft, NASA CP-3149, Proceedings of the NASA High Angle-of-Attack Technology Conference, Vol. 1, Part 2, NASA Langley Research Center, Hampton, VA, November, pp. 689-702.

Turkel, E., and Vatsa, V.N., 1994, Effect of artificial viscosity on three-dimensional flow solutions, AIAA Journal, Vol. 32, No. 1, pp. 39-45.

Zdravistch, F., and Azevedo, J.L.F., 1990, Numerical simulation of high speed flows over complex satellite launchers, 3rd Brazilian Congress of Engineering and Thermal Sciences (ENCIT), Itapema, Santa Catarina, Brazil, December.